A New Control Technique for Achieving Wide Constant Power Speed Operation with an Interior PM Alternator Machine

Jackson Wai

University of Wisconsin-Madison
1415 Engineering Drive
Madison, WI 53706
Ph: 608-265-3821
Fax: 608-262-5559
E-Mail: waij@cae.wisc.edu

Thomas M. Jahns

University of Wisconsin-Madison
1415 Engineering Drive
Madison, WI 53706
Ph: 608-262-5702
Fax: 608-262-5559
E-Mail: jahns@engr.wisc.edu

***Abstract*-A new flux weakening control algorithm is presented for achieving wide constant power operation with an interior permanent magnet (IPM) synchronous machine operating as an alternator. The algorithm is designed to initiate flux weakening only when necessary by recognizing the threshold conditions for current regulator saturation, making the algorithm inherently adaptive to changes in the inverter bus voltage. A 6kW 42V automotive integrated starter/alternator (ISA) using a direct-drive IPM machine serves as the target application for this development. Simulation results show that the new algorithm is capable of delivering very good static and dynamic bus regulation characteristics over a 10:1 engine operating speed range. Tests are presently under way to confirm these performance predictions using a prototype IPM starter/alternator system.**

Keywords: Permanent magnet machines, AC motor drives, road vehicle power systems, power control, synchronous generators

I. Introduction

With proper design, an interior permanent magnet (IPM) synchronous machine can achieve constant power operation over a wide speed range in both the motoring and generating regimes [1]. As a result, IPM machines are attracting increasing attention for a variety of applications ranging from electric vehicle propulsion [2] to machine tools [3].

While the design of an IPM machine for extended speed operation poses several technical challenges, the success of the complete drive system depends on the availability of an appropriate control algorithm that can extract the full performance capabilities from the machine. In particular, special flux weakening control techniques are necessary to achieve constant power operation over a wide speed range. Previous work reported in the literature has generally focused on extended speed range applications for the IPM machine operating as a motor [4-6]. This paper presents a new control algorithm designed to extract near-constant power from an IPM machine over a wide speed range when it is operating as an alternator.

The application that has motivated this work is a direct-drive integrated starter/alternator (ISA) for an automotive vehicle [7]. The development of many new electrically-powered accessories combined with wide interest in mild hybrid concepts using electric machines for low speed acceleration has drawn significant attention to ISA systems [8]. As illustrated in Fig. 1, the new ISA replaces the conventional engine flywheel and is driven directly by the engine crankshaft without gearing. The machine is designed to operate as both the engine starter and alternator, replacing the two separate machines that perform these functions in conventional vehicles, along with their associated pulleys, belts, and gears.

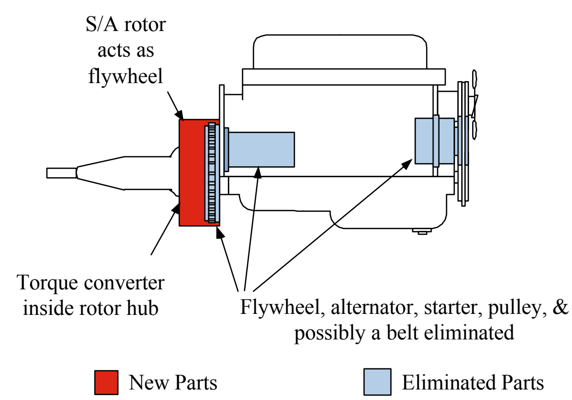

Fig. 1 Integrated starter/alternator (ISA) configuration.

Performance specifications developed in consultation with several automotive manufacturers call for the ISA to supply 150Nm of starting torque at low speeds. In addition, the ISA must deliver 42V power to the automotive accessories over a 10:1 speed range extending from 4KW at 600rpm to 6KW at 6000rpm. It is this latter requirement that motivated selection of the IPM machine for further development as an attractive candidate for this application.

Significant progress has been made towards development of an IPM machine that is capable of meeting these challenging application requirements [9]. This effort has culminated in construction of a prototype version of a 12-pole IPM machine designed for this direct-drive ISA application. Figure 2 shows the stator and rotor of this machine, illustrating its use of two magnet cavities per pole with saturating magnetic bridges that link the iron pole pieces into unitary rotor laminations.

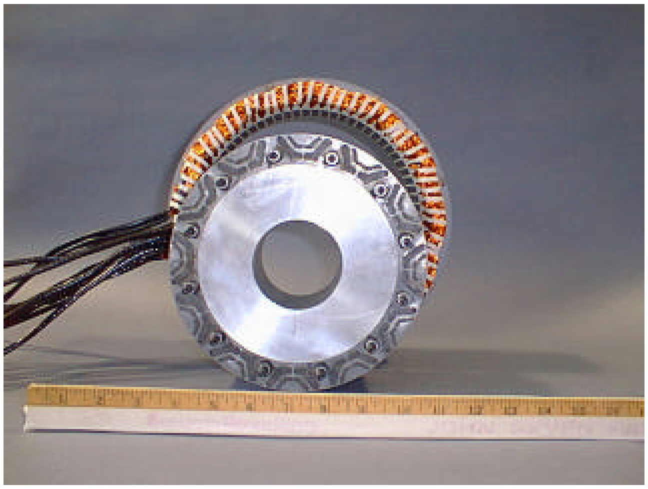

Fig. 2 Rotor and stator assemblies of prototype 6 kW IPM machine for ISA application.

II. Control Technique Presentation

A. IPM Machine Operating Envelope

The principles for achieving wide constant power operation using IPM synchronous machines have been established in the technical literature [4,10]. The machine equations governing the dynamic operation of the IPM machine in the rotor *dq* reference frame are summarized below. Note that the *d*-axis is aligned with the rotor permanent magnet flux.

$$v_d = r_s\, i_d + p\, l_{ds} - w_r\, l_{qs} \tag{1}$$

$$v_q = r_s\, i_q + p\, l_{qs} + w_r\, l_{ds} \tag{2}$$

$$l_{ds} = L_{ds}\, i_d + f_{pm} \tag{3}$$

$$l_{qs} = L_{qs}\, i_q \tag{4}$$

where

i_d and i_q are the *d*- and *q*-axis stator currents [*A*]

v_d and v_q are the *d*- and *q*-axis stator voltages [*V*]

l_{ds} and l_{qs} are the *d*- and *q*-axis stator flux linkages [*Wb*]

L_{ds} and L_{qs} are the *d*- and *q*-axis stator inductances [*H*] (Note that $L_{qs} > L_{ds}$ in an IPM machine)

f_{pm} is the *d*-axis permanent magnet flux linkage [*Wb*]

w_r is the rotor rotation frequency [*elec. rad/s*]

Magnetic saturation has a significant impact on the operating characteristics of an IPM machine. Experience with the automotive ISA machine [9,11] has indicated that saturation can be modeled quite accurately by making L_{qs} a function of the *q*-axis stator current i_q while treating L_{ds} as a constant. Cross-coupling saturation effects [12] between the *q*- and *d*-axes are not significant in this machine and are not included in this model.

Equations (1) and (2) can be rewritten using (3) and (4) plus chain differentiation to reflect the fact that L_{qs} is a function of i_q:

$$v_d = r_s\, i_d + L_{ds}\, pi_d - w_r L_{qs}\, i_{q\,s} \tag{5}$$

$$v_q = r_s\, i_q + L_{qs}'\, pi_q + w_r(L_{ds}\, i_d + f_{pm}) \tag{6}$$

where

$$L_{qs}' = \frac{\P L_{qs}}{\P i_q}\, i_q + L_{qs} \tag{7}$$

Previous work [4,10] has demonstrated the value of the *dq* current plane for evaluating the extended speed operating characteristics of IPM machines. More specifically, such plots provide a means of visually depicting the constraints imposed by the inverter voltage and current limits and their interactions. Figure 3 presents the *dq* current plane plot for the ISA machine described above whose electrical parameters are provided in the Appendix. The Appendix includes a numerical expression for L_{qs} as a function i_q that has been fit to machine's inductance characteristics.

The current limit manifests itself in Fig. 3 as a circle of amplitude 326A (peak) centered at the origin, while the voltage limit takes the form of a family of nested ellipses all centered at the IPM machine's characteristic current value, $-f_{pm}/L_{ds}$. The radii of the ellipses vary inversely with the rotor speed. These ellipses are distorted in the vertical (i_q) direction because of L_{qs} saturation effects, and their longest diameters exhibit a noticeable counter-clockwise tilt from the horizontal (i_d) axis because of stator resistance effects. At any given speed, the IPM machine can operate at any combination of i_q and i_d values that falls within the overlapping area of the current limit circle and the voltage limit ellipse associated with that speed.

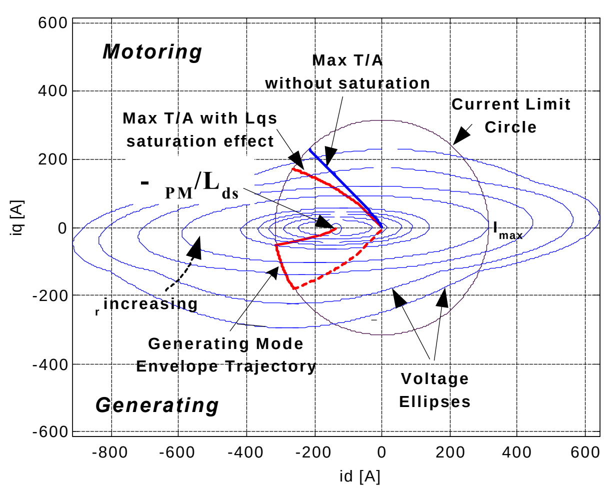

Fig. 3 Plot of i_d-i_q current plane for the 6kW IPM machine showing current limit circle, voltage limit ellipses, and current vector trajectories.

Figure 3 identifies the maximum torque-per-Amp current vector trajectory for the ISA machine in the second quadrant motoring regime for starting operation, with and without the effects of magnetic saturation. The trajectory without saturation forms an angle with the negative $-i_d$ axis that exceeds 45 degrees, while the angle of the corresponding trajectory with saturation is less than 45 degrees.

During generating operation of the IPM machine at elevated speed, the maximum output power point follows the periphery of the current limit circle towards the negative i_d axis as indicated in Fig. 3. This motion is forced by the increasing speed that progressively shrinks the voltage limit ellipse, preventing the machine from operating in the vicinity of the maximum torque-per-Amp trajectory (for generating) identified by a dashed line in Fig. 3.

The amplitude of the ISA machine's characteristic current, f_{pm}/L_{ds} (=135A) is less than the inverter current limit (326A). This may seem surprising since optimum extended speed operation occurs when the value of f_{pm}/L_{ds} equals the inverter current limit [1]. However, the other ISA system specifications, including a limit on the machine's maximum back-emf amplitude, result in this lower value of characteristic current. Given this situation, the maximum generating output power trajectory eventually separates from the current limit circle as the speed increases, following a trajectory that leads to the $-f_{pm}/L_{ds}$ characteristic current point on the negative i_d axis at infinite speed.

It is important to note that the illustrated generating mode trajectory in Fig. 3 for speeds above the corner point actually represents an optimistic outer limit for the current vector locus that can only be approached but never quite reached for an actual current regulated drive. This is true because the outer boundary of the voltage ellipse at any speed corresponds to six-step voltage operation, representing a condition in which the current regulator loops are completely saturated. Since the current regulator loses control of the instantaneous machine phase currents under such conditions [4], the current vector command must be continually adjusted so that it always resides safely *inside* the voltage ellipse. However, it is desirable to approach the ellipse as closely as possible under heavy load conditions in order to deliver maximum power from the IPM machine, taking full advantage of the available inverter dc bus voltage.

With this observation in mind, it is clear that angle between the commanded current vector and the negative d-axis in Fig. 3 must be reduced as the shrinking voltage ellipse progressively intrudes on the current limit circle for speeds above the corner point. This control action, illustrated in Fig. 4, provides the basis for the new generating mode control algorithm described in the next section.

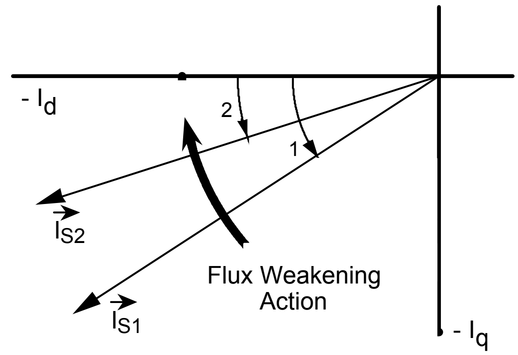

Fig. 4 Plot of current vectors illustrating flux weakening action during generating mode operation.

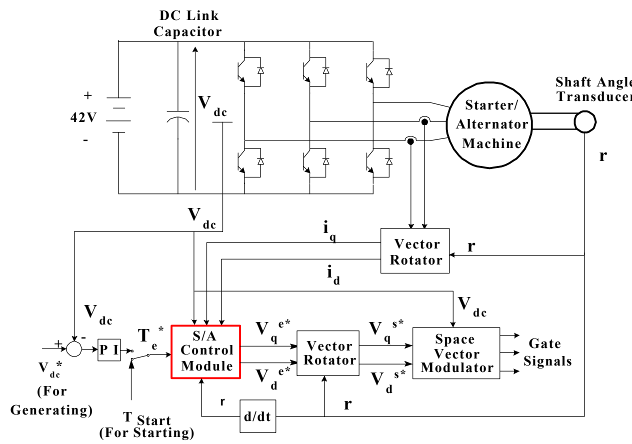

Fig. 5 Block diagram of ISA controller configuration.

B. Controller Configuration

A top-level block diagram of the ISA controller is provided in Fig. 5. This figure includes many of the features that typically appear in high-performance vector control configurations utilizing synchronous-frame current regulation. That is, phase current information is combined with rotor position feedback to develop measurements of the instantaneous i_d and i_q that are fed to the current regulator imbedded in the block labeled *S/A Control Module*. Another input to this module is the torque command T_e^* that is derived from either the starting torque command or the bus voltage regulator, depending on the system's operating mode.

The outputs of this module are the voltage commands v_d^{e*} and v_q^{e*} in the synchronous reference frame. These voltage commands are then converted back to the stationary reference frame using a second vector rotator before being applied to a space vector modulator. This modulator develops the inverter switching commands, making use of the measured bus voltage v_{dc} to insure a smooth transition from PWM operation into saturated six-step voltage operation under all bus voltage conditions [13].

Figure 6 shows the detailed structure of the *S/A Control Module* that appears as a block in Fig. 5. The control components enclosed by the inner dashed-line box in the lower half of Fig. 6 are responsible for flux weakening operation and only are activated at elevated speeds when the current vector approaches the prevailing voltage limit ellipse at any given speed. Under all other conditions, such as low-speed starting operation, the flux-weakening controller is essentially dormant, having no effect on the control action of the Fig. 6 *S/A Control Module*. The control elements lying across the top half of Fig. 7 dominate its response under such conditions, as described below.

Starting Operation

The vector control principles for controlling the ISA machine to deliver high starting torque (up to 150 Nm) as a motor are well established in the literature [14] and will be summarized only briefly here. Since starting mode operation occurs only at low speeds where the voltage limit ellipse is not a factor, the maximum torque-per-Amp trajectory in the second quadrant provides the preferred operating points for motoring torque production. The maximum available starting torque from the ISA machine occurs at the point in the second quadrant where the maximum torque-per-Amp trajectory intersects the current limit circle.

The *S/A Control Module* in Fig. 6 executes this starting mode control by converting a starting torque command T_e^* into the corresponding values of *d*- and *q*-axis current commands, i_d^m and i_q^m, using the function blocks f_1 and f_2 and the polar-to-rectangular conversion block. These *f*-functions are pre-programmed with the maximum torque-per-Amp trajectory that matches the IPM machine's characteristics. The two *f*-functions develop the desired current vector trajectory in polar coordinates as current amplitude $|I|^*$ and angle $q*$ commands (see Fig. 5) for convenient compatibility with the flux weakening control algorithm that will be described in the next section. The $q*$ angle command passes through to the polar-to-rectangular converter unaffected by the flux weakening control algorithm at low speeds during starting.

The upper right side of Fig. 6 represents the stator current regulator in the synchronous reference frame. There are many different ways in which such a regulator can be implemented. The particular implementation shown in Fig. 6 applies feedforward decoupling compensation to the output voltage commands using the machine's steady-state voltage relations, so that:

$$v_q^{ss} = r_s\, i_q^m + w_r\,(L_{ds}\, i_d^m + f_{PM}) \tag{9}$$

$$v_d^{ss} = r_s\, i_d^m - w_r\,(L_{qs}\, i_q^m) \tag{10}$$

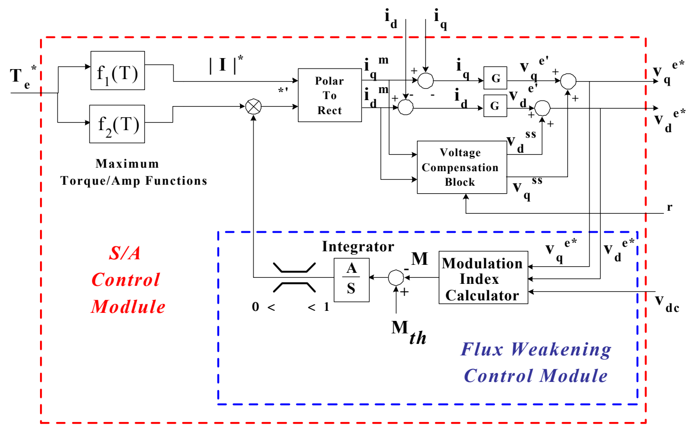

Fig. 6 Block diagram of *S/A Control Module*.

Generating Operation

Development of an effective flux-weakening control algorithm provides the key to achieving extended constant-power operation to meet the demanding generating mode requirements of the automotive ISA application. The new algorithm implemented in this system works by directly reducing the angle q of the commanded current vector with respect to the negative *d*-axis as illustrated earlier in Fig. 4.

The control elements that implement this flux weakening action are enclosed in the sub-block labeled *Flux Weakening Control Module* in the lower half of Fig. 6. This module executes the current vector angle reduction by multiplying the angle command q^* from maximum torque-per-Amp function f_2 by a scaling factor b^* that varies between 0 and 1. According to this approach, only the angle of the current vector, and not its amplitude, is directly controlled by the flux weakening algorithm. As long as the value of b^* is 1, the *Flux Weakening Control Module* exerts no influence on the current vector trajectory defined by the maximum torque-per-Amp trajectory.

The value of b^* is determined by how closely the required stator voltage approaches the saturated six-step voltage value at any instant in time. Since the ISA drive is designed for high frequency PWM operation, the instantaneous PWM modulation index, M, can be used as a convenient and sensitive indicator of the current regulator's proximity to total saturation (i.e., $M = 1$). The modulation index value can be conveniently calculated using the synchronous frame *dq* voltage commands, v_{qs}^{e*} and v_{ds}^{e*}, as follows:

$$M = \frac{\sqrt{(v_{ds}^{e*})^2 + (v_{qs}^{e*})^2}}{\frac{2}{p} V_{dc}} \tag{11}$$

where V_{dc} is the measured value of the dc link voltage at the converter input terminals.

Any excess value of M above a preset threshold level, M_{th} (less than but close to 1) is integrated to reduce the value of b^* ($0<b^*<1$) that scales the current vector command angle according to $q^{*'} = b^* \cdot q^*$. This feedback loop achieves the desired flux weakening action in Fig. 4 by swinging the current vector in towards the negative d-axis in order to retain it within the prevailing voltage ellipse at that time instant. By this action, the value of the modulation index naturally decreases as the current vector operating point moves away from the voltage ellipse boundary, establishing a stable operating point loop in the flux weakening regime.

When the torque command and/or rotor speed drop sufficiently so that flux weakening is no longer required, the feedback loop naturally responds accordingly to reduce its effect on the current vector angle q. That is, the value of b^* quickly integrates back to 1 when the modulation index drops below its threshold value M^*. Thus, the feedback loop becomes passive with no effect on the vector control operation until flux weakening action is required again.

Use of the measured value of dc link voltage V_{dc} in the modulation index calculation (11) makes it possible for the controller to adapt immediately to any changes in the bus voltage. This feature is important in applications such as an automotive ISA where the dc bus voltage can be expected to change significantly depending on the bus loading and the vehicle battery state of charge. On the other hand, this voltage measurement can be replaced by a constant value in applications where the dc bus voltage is known and well regulated within a narrow range, eliminating the need for the bus voltage sensor.

The flux weakening algorithm introduced above is naturally bipolar, working as well for motoring operation as for generating where it is primarily needed in the ISA application. The resulting motoring torque envelope along the voltage ellipse boundary for the IPM machine in this ISA application is shown in Fig. 7. This figure confirms that the required 150 Nm for starting will be available at low speeds during operation on the maximum torque-per-Amp trajectory.

IV. Controller Performance

A. Drive System Simulation

Steady-state and dynamic performance characteristics of the complete ISA drive system including the machine, PWM inverter and the controller have been investigated using computer simulation. Matlab/Simulink™ was chosen as the preferred simulation software tool for carrying out this analysis.

The switching behavior of the inverter is modeled using six ideal switches. The IPM machine is modeled in the dq synchronous frame using the parameter values found in the Appendix, including the effects of magnetic saturation on L_{qs} as a function of i_q. All of the controller functions are

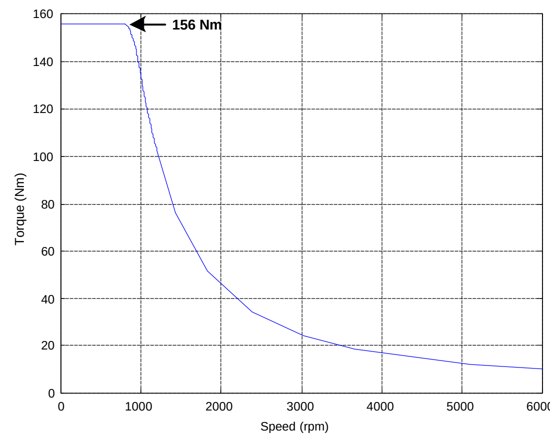

Fig. 7 Motoring torque envelope for the ISA machine operating with a 42V bus.

modeled individually including PWM space vector modulation and its saturation characteristics as the modulation index M approaches 1. However, controller quantization and sampling delays have not been included in this model.

Starting Mode Operation

Simulation results confirm that the ISA drive system operates as expected to deliver 150 Nm during low-speed starting operation. Since the engine is designed to start at speeds well below 500 rpm, flux weakening operation is not activated during this operating mode.

Dynamic specifications for the ISA starting mode operation call for development of full starting torque within 20 ms, based on suggestions from automaker representatives who have helped to oversee this development effort. Figure 8 shows the simulated step torque response of the IPM machine at standstill using a nominal 42 Vdc bus voltage. The torque response curve predicts that the system response to such a large-signal step command is very well behaved, with the torque reaching its final value of 150 Nm within 5 ms, far less than the 20 ms maximum limit. Once reached, the system holds the steady-state torque very stably at the desired 150 Nm level as the machine rotor accelerates.

According to draft specifications that have been developed for the new 42-V bus [15], the bus voltage is allowed to temporarily drop as low as 21 V during starting mode operation due to the heavy electrical load. Simulation of starting mode operation with the bus voltage set at 21 V (see Fig. 9) confirms that the IPM machine retains its capability of developing the required 150 Nm well within the 20 ms dynamic response requirement. The machine corner speed drops to approximately 400 rev/min under these low bus voltage conditions (refer to Fig. 7), but this corner speed is still sufficiently high to insure fast engine starting.

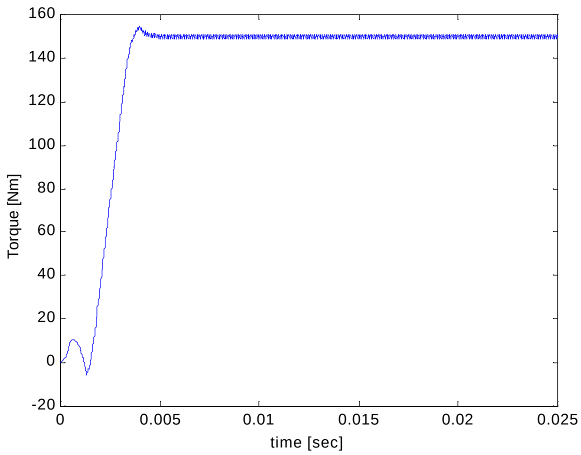

Fig. 8 Starting torque step response for 150 Nm command. V_{dc} = 42V

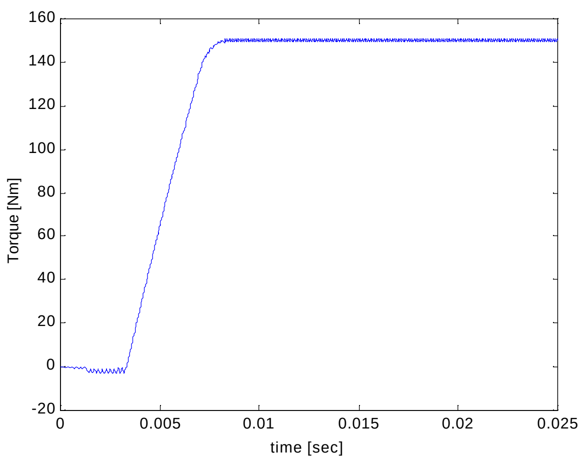

Fig. 9 Starting torque step response for 150 Nm command. V_{dc} = 21V

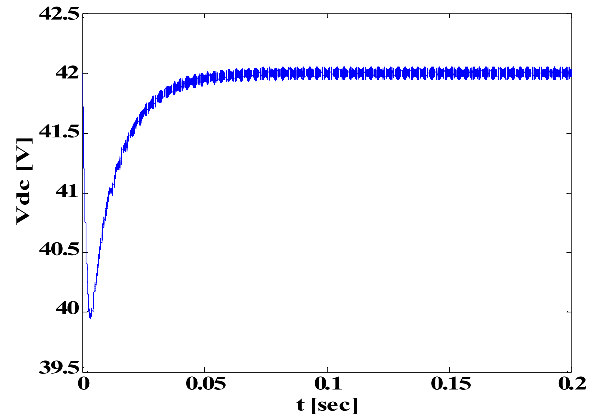

Fig. 10 Generating mode bus voltage response for step load increase from 0 to 4kW at 600 rev/min. *Note expanded scale and suppressed zero.*

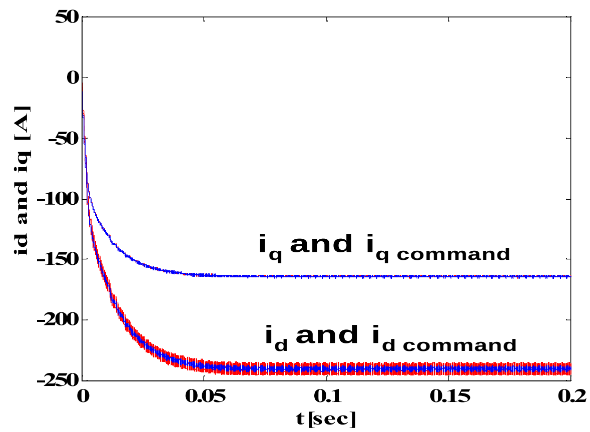

Fig. 11 Generating mode *d*- and *q*-axis current commands and responses for step load increase from 0 to 4kW at 600 rev/min.

Generating Mode Operation

Based on the emerging specifications for the new 42-V Powernet [15], the bus voltage should be regulated to remain within a band of voltage between 30 and 50 V during normal operation. A simple closed-loop voltage regulator using the measured bus voltage was introduced into the system during ISA system operation in the generating mode, as indicated in Fig. 5.

The Simulink ISA system model has been used to evaluate the performance capabilities of this generating mode controller under various operating conditions. Unlike the starting mode operation described above, system operation as an alternator inevitably exercises the new flux weakening algorithm, particularly at higher speeds.

It is assumed that a 42-V battery is connected to the bus to supply the engine starting power as indicated in Fig. 5. In addition, a dc link capacitor is present to absorb the PWM ripple current from the switching converter as well as to assist in supporting the bus voltage during transient loading. The battery has been modeled as a voltage source in series with a resistance. Parameters for a charged lead-acid battery were used to maximize the resistive decoupling between the battery and the ISA system (see Appendix).

Figures 10 and 11 present the predicted transient response characteristics of the ISA system during generating mode operation for a sudden step in load from 0 to 4 kW (i.e., rated load) at 600 rev/min. This represents a worst-case step load that exceeds any transients expected during

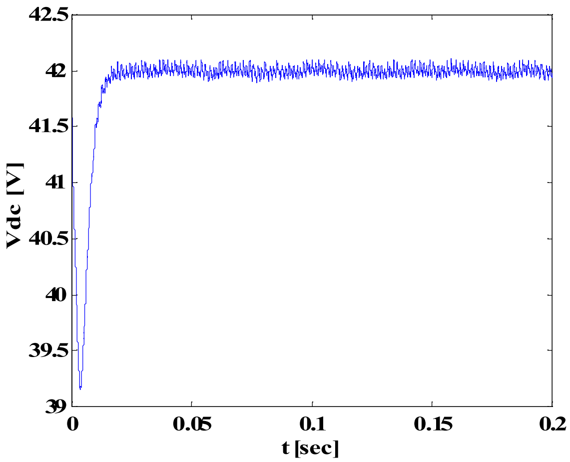

Fig. 12 Generating mode bus voltage response for step load increase from 0 to 6kW at 6000 rev/min.

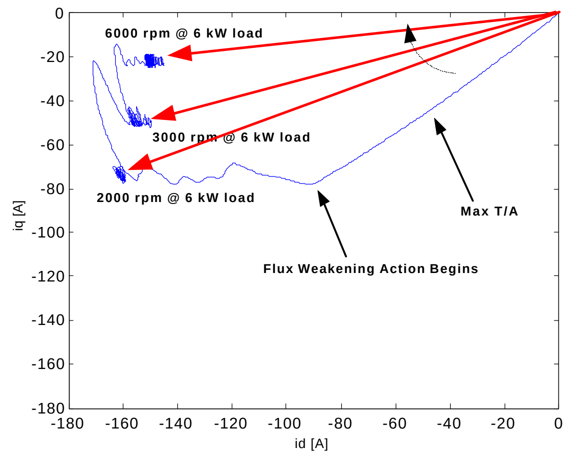

Fig. 14 Transient current vector trajectory during steps from 0 to 6kW at 2000 rev/min, followed by stepped speed increases to 3000 rev/min and then to 6000 rev/min, all at 6 kW.

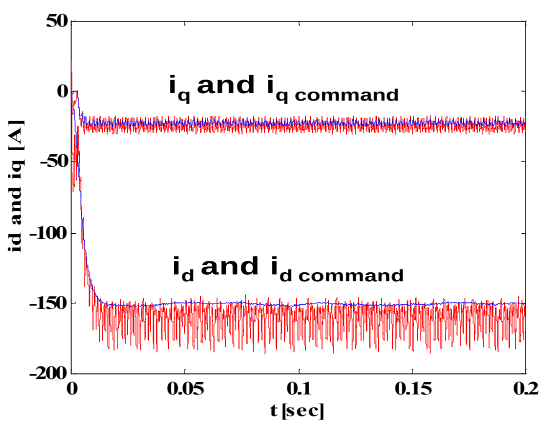

Fig. 13 Generating mode *d*- and *q*-axis current commands and responses for step load increase from 0 to 4kW at 600 rev/min.

normal vehicle operation. The bus voltage recovers to 42 V in approximately 50 ms with a maximum voltage excursion of 2 V, well within the specified limits for normal Powernet operation (note the expanded scale and suppressed zero in Fig. 10). The *d*- and *q*-axis currents in Fig. 11 are similarly well behaved, rising smoothly from 0 to their new steady-state values needed to support the 4 kW load.

Figures 12 and 13 show the corresponding transient responses for the bus voltage and *dq* machine currents during a worst-case step load from 0 to 6 kW (rated load) at the maximum operating speed of 6000 rev/min. Although the transient voltage dip is somewhat larger (2.8V) than for the 4 kW step, the duration of the transient is noticeably shorter (~15 ms). Here again, all of the transient waveforms are well behaved. Because of the high speed, the 6kW operating point takes the IPM machine deep into its flux weakening regime. This is apparent from the post-transient steady-state current values in Fig. 13, with large negative values of i_d compared to i_q.

The action of the flux weakening algorithm can be clearly illustrated by examining the transient trajectory of the stator current vector in the synchronously-rotating *dq* reference frame as shown in Fig. 16. In this example, the delivered output power is initially stepped from 0 to 6 kW at 2000 rev/min. The speed is subsequently stepped first to 3000 rev/min, and, finally, to 6000 rev/min with the output power held constant at 6 kW. Each of these steps takes the IPM deeper into flux weakening operation, apparent in Fig. 14 from the clockwise migration of the current vector in the direction of the negative *d*-axis.

B. Experimental Verification

A demonstrator version of the ISA system using the prototype IPM synchronous machine shown earlier in Fig. 2 has been assembled for purposes of experimental verification. A block diagram of this equipment is provided in Fig. 15. Since the focus of this verification effort is on the machine and the controller, the inverter power stage of a commercial industrial drive (excited via a step-down transformer to generate the 42V dc link) was selected for use in the ISA drive system. The control algorithm has been implemented using a dSpace 1103 controller, appropriate for this type of rapid prototyping effort. A high-performance four-quadrant induction motor drive is used as the load machine and prime mover during ISA starter and alternator operation, respectively.

Experimental tests are planned to verify the operating characteristics of the ISA system, including the performance of the flux weakening control algorithm during generating mode operation. Results of this testing will be presented at the conference.

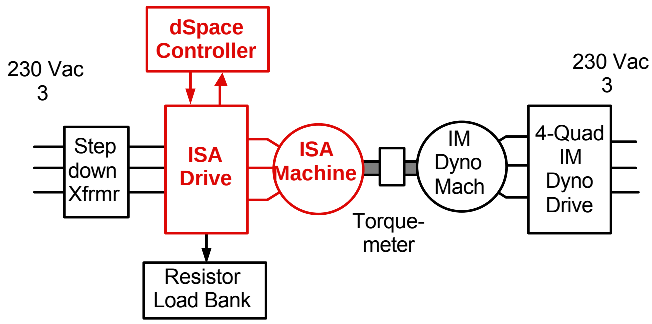

Fig. 15 Laboratory configuration for ISA system tests.

V. Conclusions

This paper has presented a new flux weakening algorithm for an IPM synchronous alternator machine suitable for exciting the machine to deliver constant power over a wide speed range (10:1 or higher). The flux weakening algorithm acts to rotate the instantaneous current towards the negative *d*-axis in the synchronously-rotating reference frame in order to establish and maintain operation within the combined constraints imposed by the available voltage, current, and the rotor speed. Advantages of this algorithm include its ability to automatically adapt to changes in the bus voltage by using the PWM modulation index to recognize the threshold of current regulator saturation.

Simulation results have been presented that demonstrate the desirable performance characteristics of this algorithm over a wide speed range in conjunction with an automotive integrated starter/alternator system designed to deliver 6kW at 6000 rev/min. The results indicate that the flux weakening algorithm responds rapidly and in a well-behaved manner over a wide range of operating conditions. Experimental tests are presently being conducted to confirm these predicted results.

Appendix

Machine Parameters

$R_s = 0.0103$ $L_{ds} = 64.97$ H $f_{PM} = 6.3\text{x}10^{-3}$ Wb

$L_{qs} = C\,(i_{qs})^B$ [H] for $L_{qs} < L_{qmax}$; otherwise $L_{qs} = L_{qmax}$

where $C = 0.0058$, $B = -0.605$, $L_{qmax} = 305.05$ H

Lead-Acid Battery Model(Charged) and dc Link Parameters

$V_{bat} = 38.9$ V $R_{bat} = 10$ $C_{bus} = 75\text{x}10^{-3}$ F

Acknowledgments

The authors gratefully acknowledge the support of the MIT Consortium on Advanced Automotive Electrical/Electronic Components and Systems and the Wisconsin Electric Machines and Power Electronics Consortium (WEMPEC). We also thank Dr. Edward Lovelace for his generous consultation assistance regarding the ISA machine.

References

[1] W.L. Soong, “Theoretical Limitations to the Field-Weakening Performance of the Five Classes of Brushless Synchronous AC Motor Drives”, *Proc. IEE Elec.Machines & Drives Conf*, 1993, Oxford, England, pp. 127-132.

[2] J-W Park, K-H Koo, J-M Kim, “Improvement of Control Characteristics of Interior Permanent Magnet Synchronous Motor for Electric Vehicle”, *Rec. of Ind. Appl. Soc. Ann. Mtg*, Rome, 2000, pp. 1888-1895.

[3] A. Fratta, A.Vagati, F. Villata, "On the Evolution of AC Machines for Spindle Drive Applications", *Rec. of IEEE Ind. Appl. Soc. Ann. Mtg*., 1989, pp. 699-704.

[4] T.M. Jahns, “Flux Weakening Regime Operation of an Interior Permanent-Magnet Synchronous Motor Drive”, *IEEE Trans. on Ind. Appl.*, vol. IA-23, no. 4, pp. 55-63, 1987.

[5] J.Kim, S. Sul, "Speed Control of Interior PM Synchronous Motor Drive for the Flux-Weakening Operation," *IEEE Trans. Ind. Appl.*, vol. 33, pp. 43-48, Jan/Feb. 1997.

[6] N. Bianchi, S. Bolognani, M. Zigliotto, "High Performance PM Synchronous Motor Drive for an Electric Scooter", *Rec. of Ind. Appl. Soc. Ann. Mtg*, Rome, 2000, pp. 1901-1908.

[7] E.C. Lovelace, T.M. Jahns, J.L. Kirtley Jr. and J.H. Lang, “An Interior PM Starter/Alternator For Automotive Applications” in *Proc. of Intl Conf. on Elec. Machines*, 1998, Istanbul, Turkey, pp. 1802-1808.

[8] J.G. Kassakian, J.M. Miller, and N. Traub, ”Automotive Electronics Powers Up”, *IEEE Spectrum*, May 2000, pp. 34-39.

[9] E.C. Lovelace, “Optimization of A Magnetically Saturable Interior Permanent-Magnet Synchronous Machine Drive”, PhD Thesis, Dept. of Electrical Eng. and Computer Science, M.I.T., 2000.

[10] S. Morimoto, Y. Takeda, T. Hirasa, K. Taniguchi, “Expansion of Operating Limits for PM Motor by Current Vector Control Considering Inverter Capacity, *IEEE Trans. on Ind. Appl*., vol. 26, pp. 920-926, Sept/Oct 1990.

[11] E. Lovelace, T. Jahns, J. Lang, "A Saturating Lumped Parameter Design Model for an Interior PM Synchronous Machine", *Proc. of IEEE Intl. Elec. Machines & Drives Conf.*, 1999, Seattle, pp. 553-55.

[12] A. Vagati and G. Franceschini, “Cross-Saturation in Synchronous Reluctance Motors of the Transverse-Laminated Type”, *Rec. of IEEE Ind. Appl. Soc. Ann. Mtg.*, 1998, pp. 127-135.

[13] J. Holtz, W. Lotzkat, and A. Khambadkone, “On Continuous Control of PWM Inverters in the Overmodulation Range with Transition to the Six-step Mode”, *in Proc. of IEEE Ind. Elec. Conf*., 1992, San Diego, pp. 307-312.

[14] T. Jahns, G. Kliman, and T. Neumann, “Interior PM Synchronous Motors for Adjustable Speed Drives”, *IEEE Trans. on Ind. Appl.,* vol. IA-22, July/Aug 1986, pp. 738-747.

[15] "Road vehicles – Conditions for electrical and electronic equipment for a 42V powernet – Part 1: General", Draft specification, WGS/WD 03/2000-1, ISO, Apr 2000.